Electronic Supplementary Information for

Creating of rigid host framework with optimum crystal structure and interface for zero-strain K-ion storage

Yun-Hai Zhu,‡[ab] Jia-Zhi Wang,‡[bc] Qi Zhang,[b] Yang-Feng Cui,[bd] Gang Huang,[b] Jun-Min Yan,[a] and Xin-Bo Zhang*[bc]

[a] Key Laboratory of Automobile Materials (Jilin University), Ministry of Education, Department of Materials Science and Engineering, Jilin University, Changchun 130022, China

[b] State Key Laboratory of Rare Earth Resource Utilization, Changchun Institute of Applied Chemistry, Chinese Academy of Sciences, Changchun, 130022, P. R. China

[c] University of Science and Technology of China, Hefei, 230026, China

[d] School of Materials Science and Engineering, Changchun University of Science and Technology, Changchun 130022, China

‡ These authors contributed equally.

*Correspondence: xbzhang@ciac.ac.cn

Experimental Section

Materials Synthesis

The $KTiNbO_5$ was synthesized by heating a stoichiometric mixture of K_2CO_3, TiO_2, and Nb_2O_5 at 1100 °C for 24 h.[1] The protonated form $HTiNbO_5$ was prepared by the proton exchange reaction of 1 g $KTiNbO_5$ with 200 HCl aqueous solution (4 M) for three days.[2] After that, the withe powder was washed with distilled water and centrifuged until the supernatant was neutralized at pH 7, and then freeze-dried. The dehydrated form $Ti_2Nb_2O_9$ was produced by heating $HTiNbO_5$ at 450 °C for 1 h under air atmosphere.[3] To prepare the carbon-coated $Ti_2Nb_2O_9$ nanosheets (CTNO), 0.5 g $HTiNbO_5$ was first added to 80 mL aqueous solution containing 50 ml distilled water and 30 ml Tetrabutylammonium hydroxide solution (TBAOH, ~25% in H_2O) under magnetic stirring at room temperature. And then, the resultant solution was sonicated for 3 h, followed by magnetic stirring for another 7 days. After the exfoliation reaction, the precipitate was washed with distilled water for 5 times to remove the residual TBAOH and then freeze-dried. Finally, the as-prepared white powder was calcined at 450 °C for 1h to synthesize CTNO.

Materials Characterization

Powder X-ray diffraction (XRD) measurement was performed on a Bruker D8 Focus Powder X-ray diffractometer using Cu *Kα* radiation (40 kV, 40 mA). Field-emission scanning electron microscopy (FE-SEM) was performed on a field emission Hitachi S-4800 instrument, operating at an accelerating voltage of 10 kV. Transmission electron microscope (TEM) was performed using an FEI Tecnai G2S-Twin instrument with a field emission gun operating at 200 kV. The atomic force microscopy (AFM) was performed on Bruker Dimension Icon. X-ray photoelectron spectroscopy (XPS) spectra were obtained with an ESCALAB MK II X-ray photoelectron spectrometer using an Al *Kα* source. Raman spectra were collected with a micro-Raman spectrometer (Renishaw) with a laser of 532 nm wavelength. Thermogravimetric analysis (TG) was performed at a heating rate of 10°C min^{-1} in air atmosphere (NETZSCH STA 449F3, Germany).

Electrochemical Measurement

KTNO and TNO electrodes were prepared by mixing active material (70 wt%), acetylene black (20 wt%), and CMC (10 wt%) in water. HTNO electrodes were prepared by mixing active material (70 wt%), acetylene black (20 wt%), and CMC (10 wt%) in water (or PVDF (10 wt%) in NMP). The slurries were then uniformly spread onto copper foil, followed by drying at 100 °C in vacuum for 12 h. Coin cells (CR2025) were assembled in the Argon-filled glove box by using a K metal counter electrode and glass fiber separator. 1 M KFSI in DME was used as the electrolyte. Galvanostatic charge/discharge cycling tests were performed with a Land CT2001A battery testing system (Land, P. R. China) at a constant temperature of 25 °C.

DFT Calculation

Vienna ab initio Simulation Package (VASP) implemented with spin-polarized density functional theory (DFT) was used for all calculations.[4] The generalized gradient approximation (GGA) with the Perdew-Burke-Ernzerhofwas used to describe the electron-ion interactions was employed.[5] The surface Brillouin zone was sampled with a 4×7×2 Monkhorst-Pack mesh for primitive cell optimization and a 2×2×1 Monkhorst-Pack mesh with a cutoff energy of 500 eV for the supercell calculations. An electronic self-consistent iteration was set at 1.0×10^{-5} eV, and the forces were smaller than 0.02 eV/Å for atomic positions relaxation. The binding energy is calculated as:

$$E_b = E(K@M) - E(M) - E(K\ bulk)/n$$

Where $E(K@M)$ is the total energy of adsorbed K ion in channel of materials, $E(M)$ is the energy of materials, $E(K\ bulk)$ and n represent the energy of bulk of K metal and the number of atoms in the unit cell, respectively. Climbing image nudged elastic band method (CI-NEB) was used to search the diffusion energy barriers.[6] For CI-NEB calculations, optimization of all transition states was stopped when the forces on all images dropped below 0.03 eV/Å and 5 points were defined to form a continuous path between the reactant and the product. The frequency

calculation was used to verify the transition states. The relative reaction energy plots was obtained from optimization and transition state calculations. The electronic structure was investigated by static calculation, and different charge was calculated to determine the strength of the materials' bond with K ion.

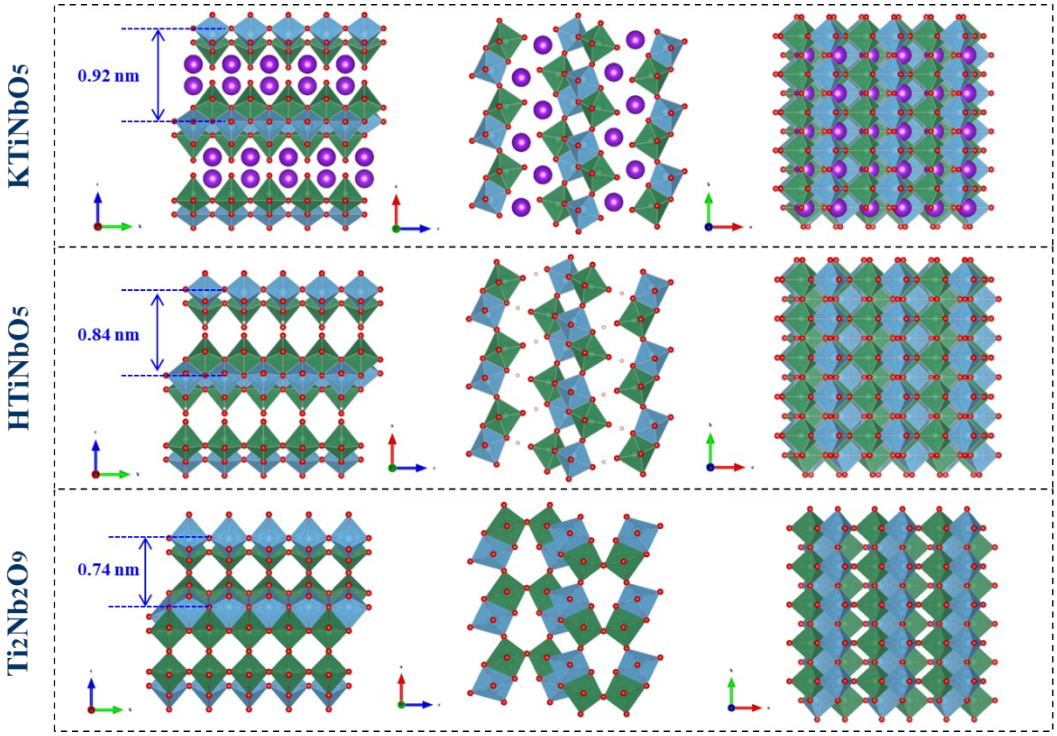

Fig. S1. Schematic illustration for the structures of KTNO, HTNO, and TNO.

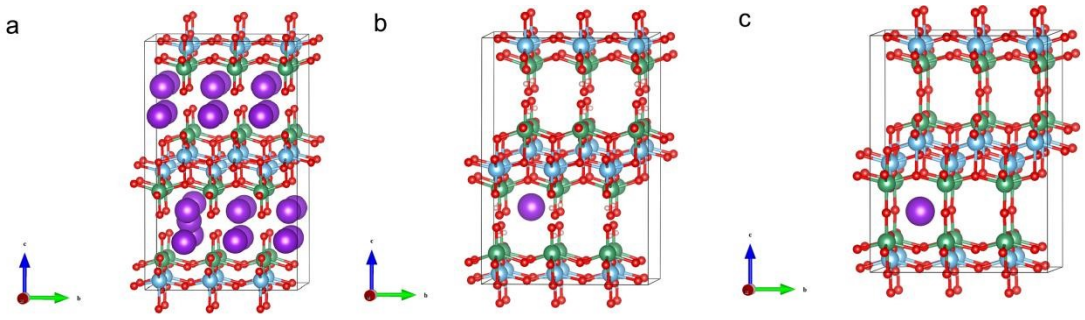

Fig. S2. The structure models for KTNO (a), HTNO (b), and TNO (c) after one K-ion insertion.

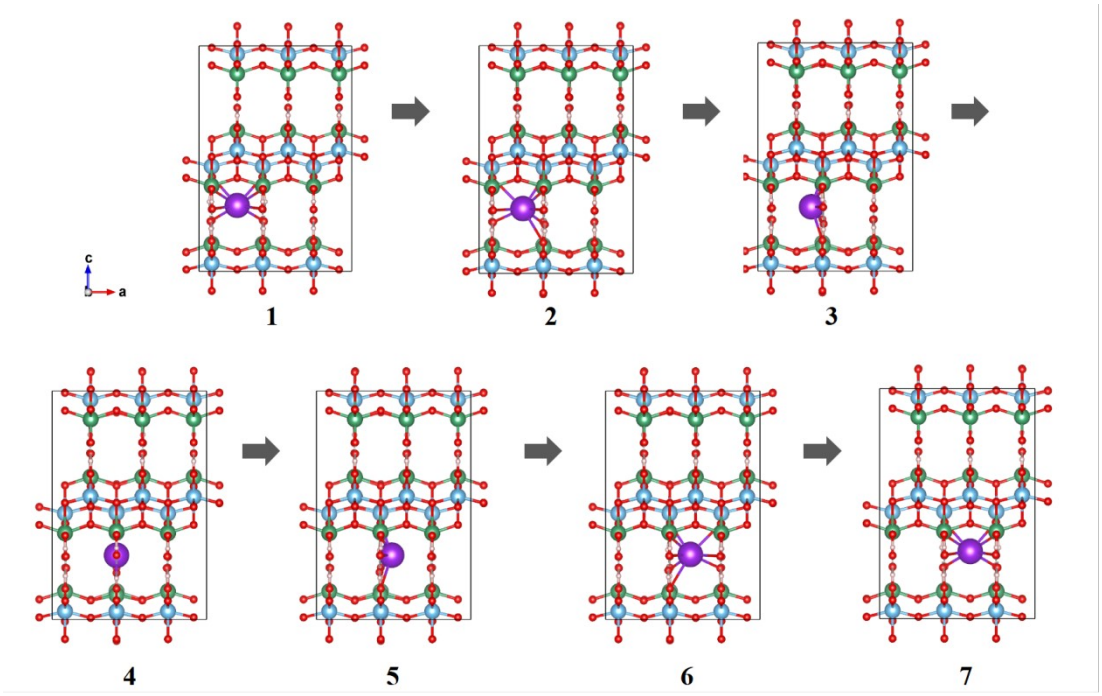

Fig. S3. The intermediate structures for the diffusion of K ion in HTNO.

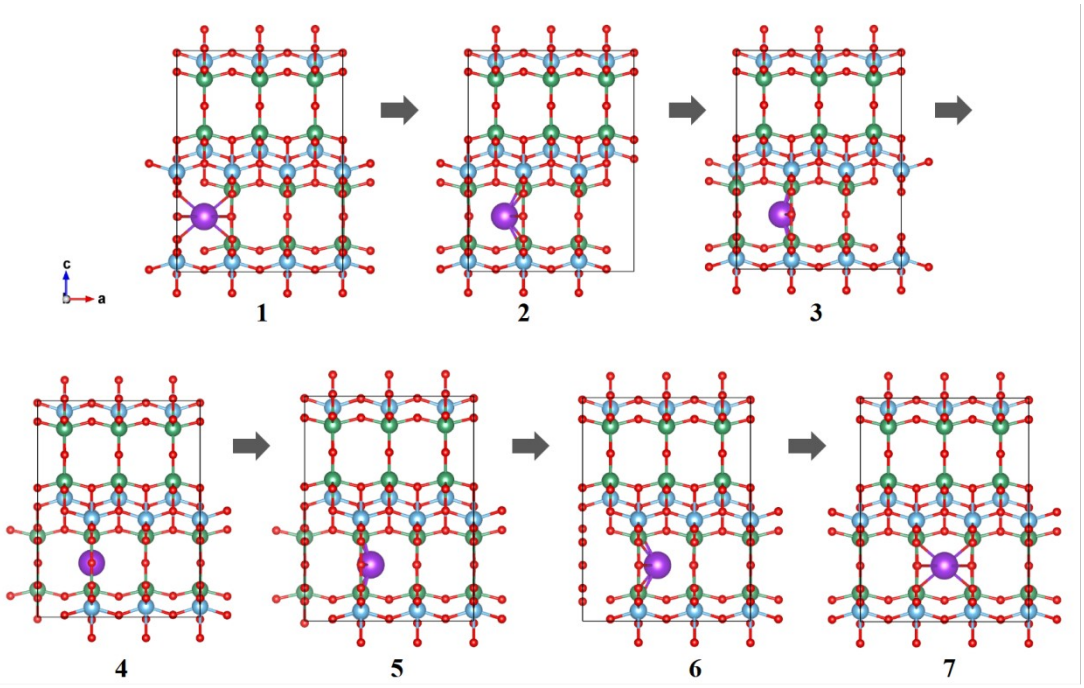

Fig. S4. The intermediate structures for the diffusion of K ion in TNO.

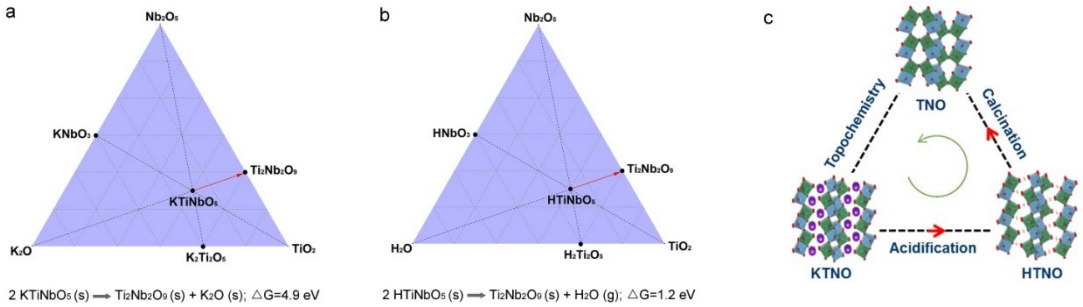

Fig. S5. (a,b) The phase diagrams for KTNO (a) and HTNO (c). (c) Schematic illustration for the topological transformations among the KTNO, HTNO, and TNO. The transformations from KTNO to TNO are with higher △G than that of from HTNO to TNO, which means that the topological dehydration of HTNO into TNO is the more feasible way to synthesize TNO.

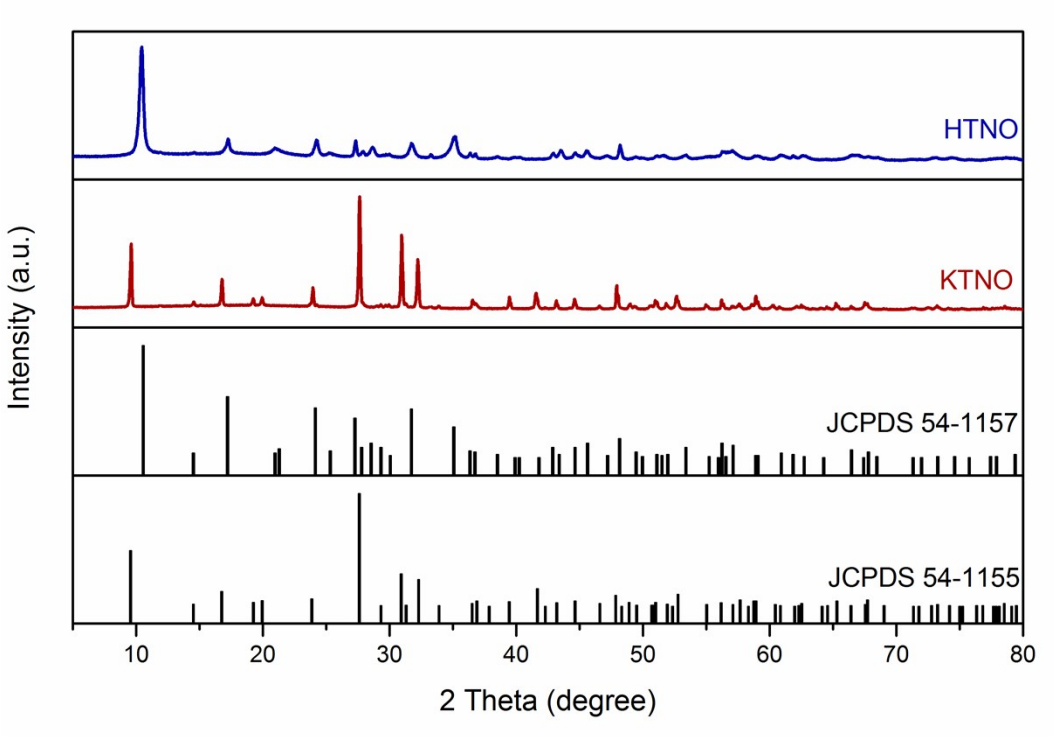

Fig. S6. XRD patterns of KTNO and HTNO.

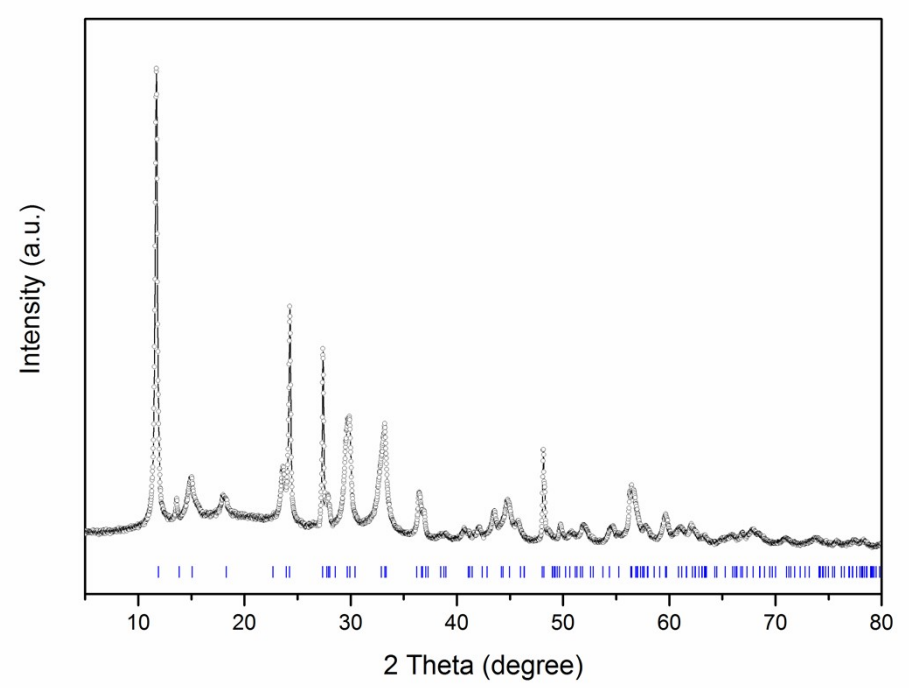

Fig. S7. XRD patterns of TNO and Bragg peaks positions for the KTi_3NbO_9 cell. The TNO possesses a three-dimensional (3D) structure with empty tunnels and is characterized by a framework similar to that of KTi_3NbO_9, so we can approximatively index the peaks with the parameters of KTi_3NbO_9.[7-9]

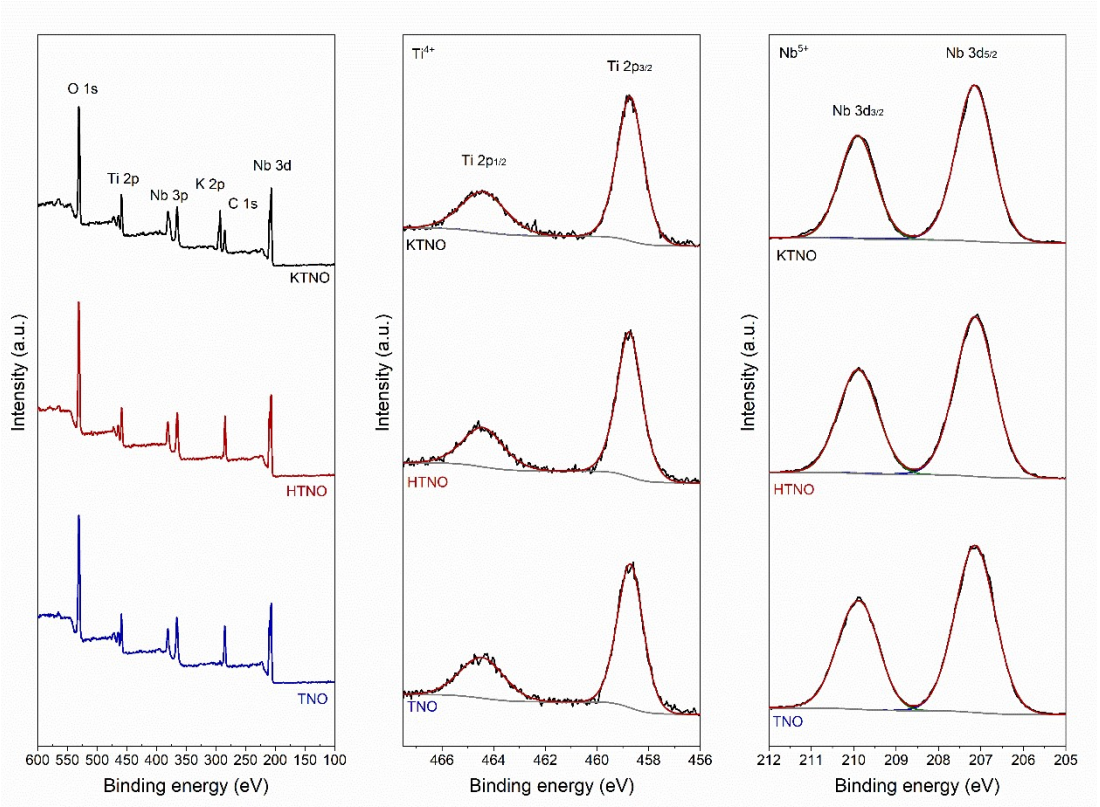

Fig. S8. XPS spectra of KTNO, HTNO, and TNO.

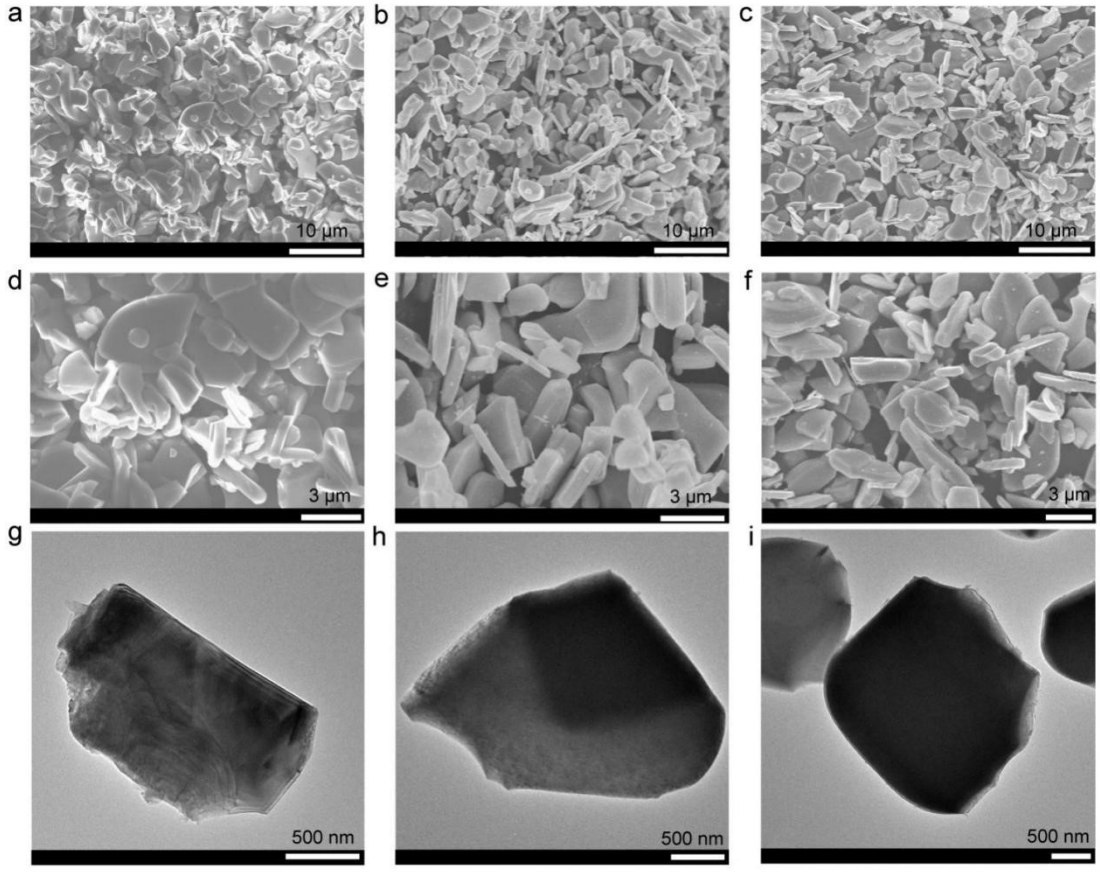

Fig. S9. SEM and TEM images of KTNO (a, d, g), HTNO (b, e, h), and TNO (c, f, i).

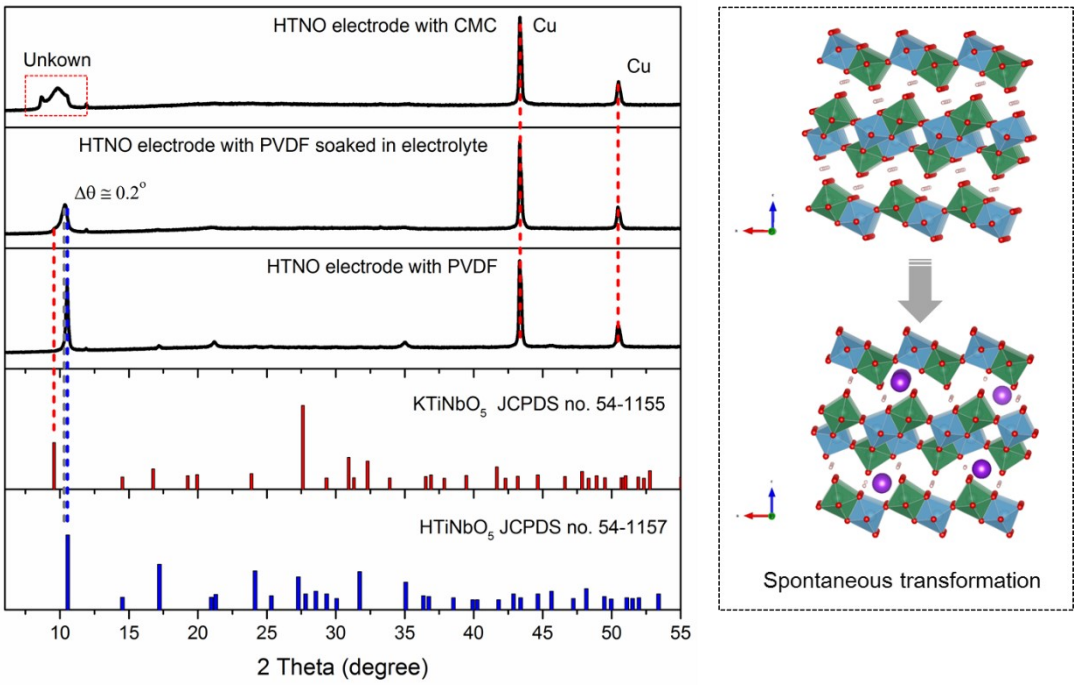

Fig. S10. XRD patterns of HTNO electrode with different treatment conditions. Note that the XRD pattern of HTNO electrode significantly changed after immerging in electrolyte for a few hours (assembly into the battery with metal K as a counter electrode) or preparation with CMC binder, which indicated the unstable structure of HTNO. Additionally, a weak peak attributed to KTNO (JCPDS no. 54-1157) was detected in the XRD pattern of HTNO electrode after being soaked in the electrode (12 h; assembly into the battery with metal K as a counter electrode), which meant a part of protons in HTNO was replaced by K ion during this process, generating KTNO, as illustrated in the right figure.

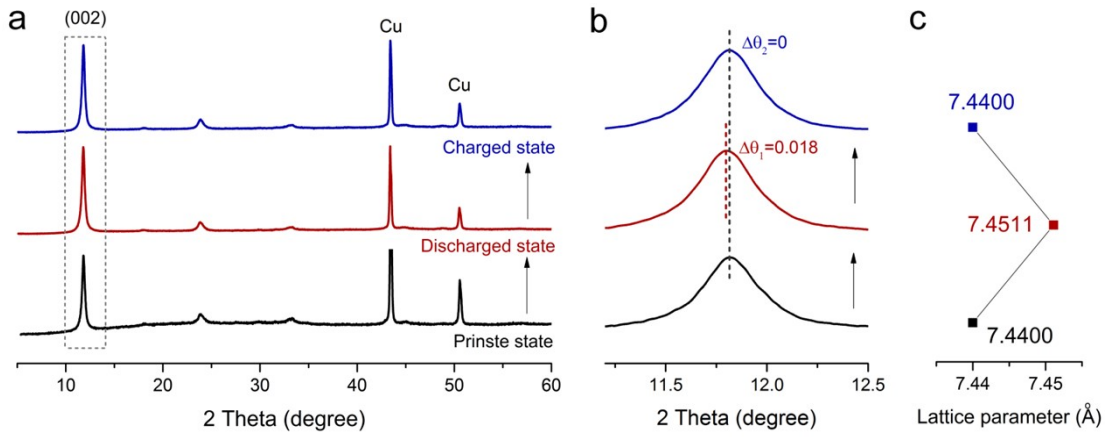

Fig. S11. XRD patterns of pristine TNO, the discharged phase at 0.01V, and the charged phase at 3 V.

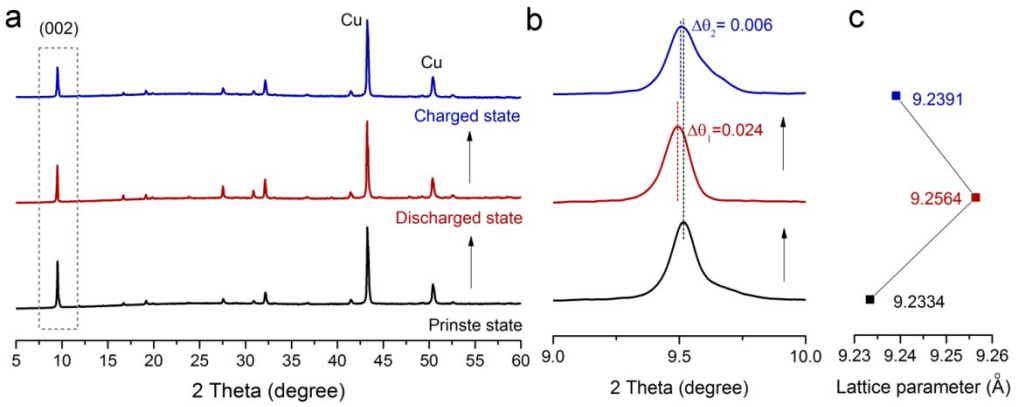

Figure S12. XRD pattern of pristine KTNO, the discharged phase at 0.01V, and the charged phase at 3 V.

Fig. S13. Photograph of KTNO, HTNO, TNO and TNO powders.

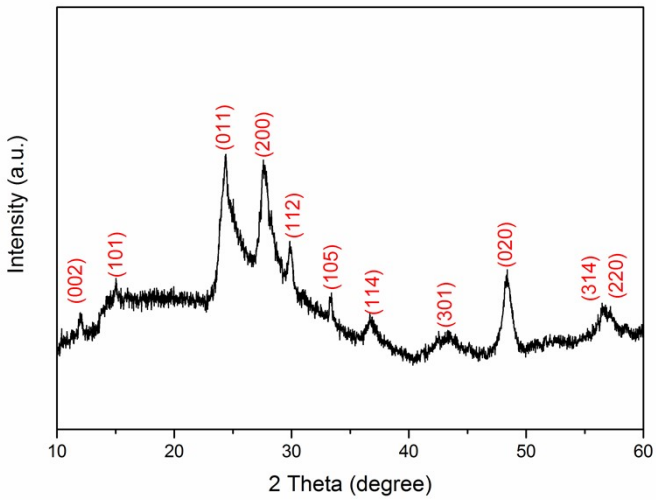

Fig. S14. XRD pattern for CTNO.

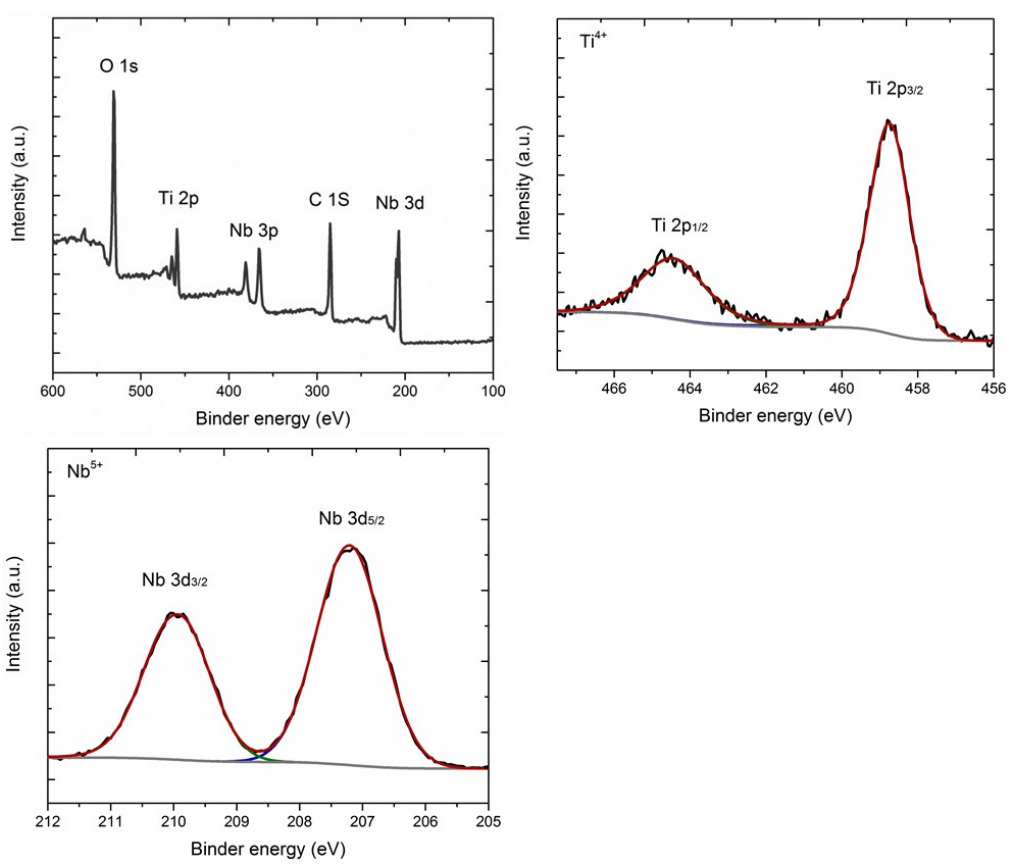

Fig. S15. XPS spectra of CTNO.

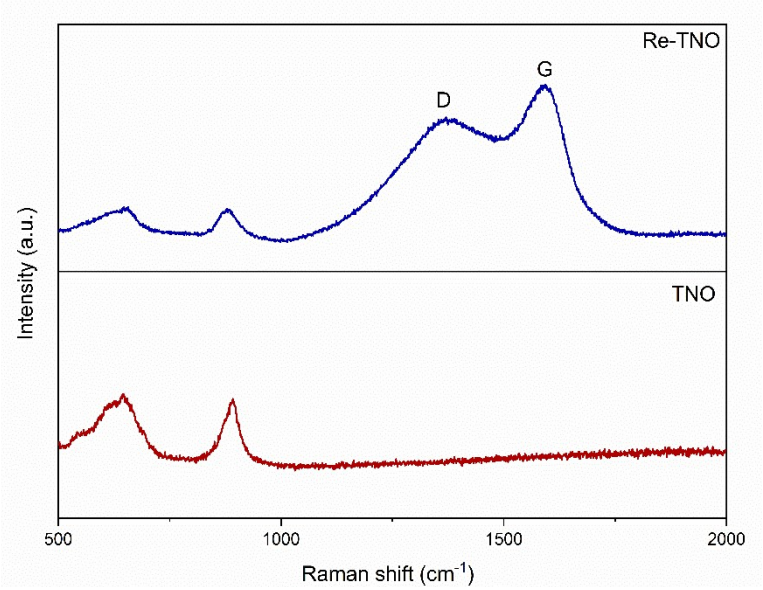

Fig. S16. Raman spectra for CTNO and TNO.

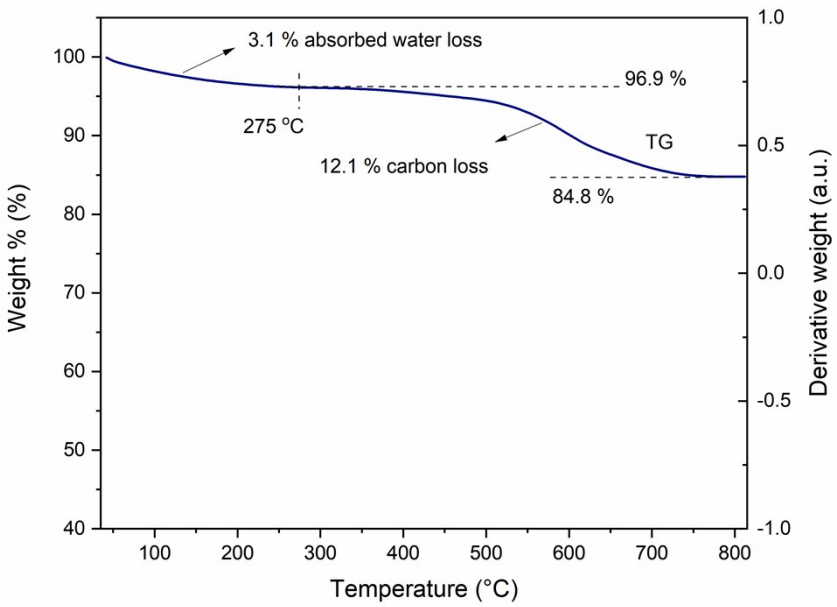

Fig. S17. TG curve of CTNO. Note that the weight loss (ca. 3.1 %) before 275 °C are corresponded to the adsorbed water loss. A rapid weight loss (ca. 12.1 %) was observed above 275 °C, which indicates the carbon oxidation. So the content of carbon in CTNO is ca. 12.5 % (12.1 % divided by 96.9 %).

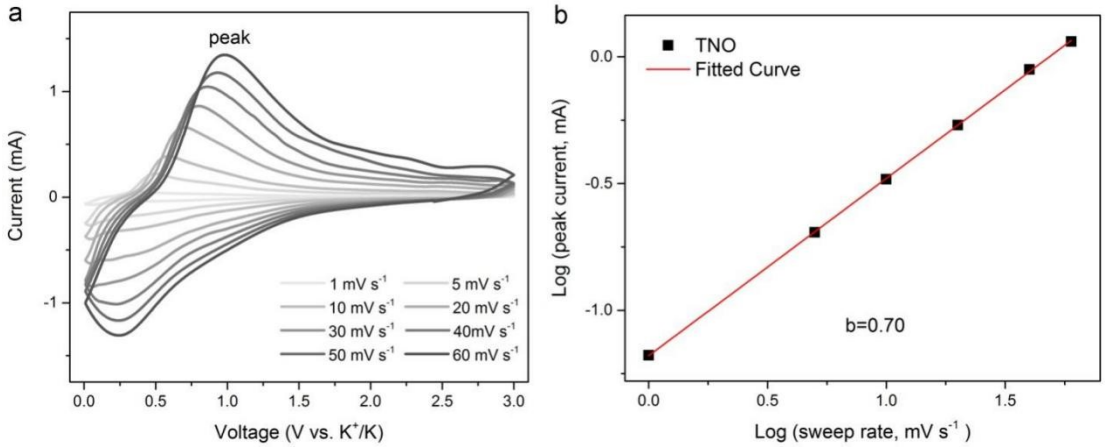

Fig. S18. (a) CV curves of TNO at various scan rates from 1 to 60 mV s^{-1}. (b) Calculation of b-values from the relationship between the scan rate and peak current in A.

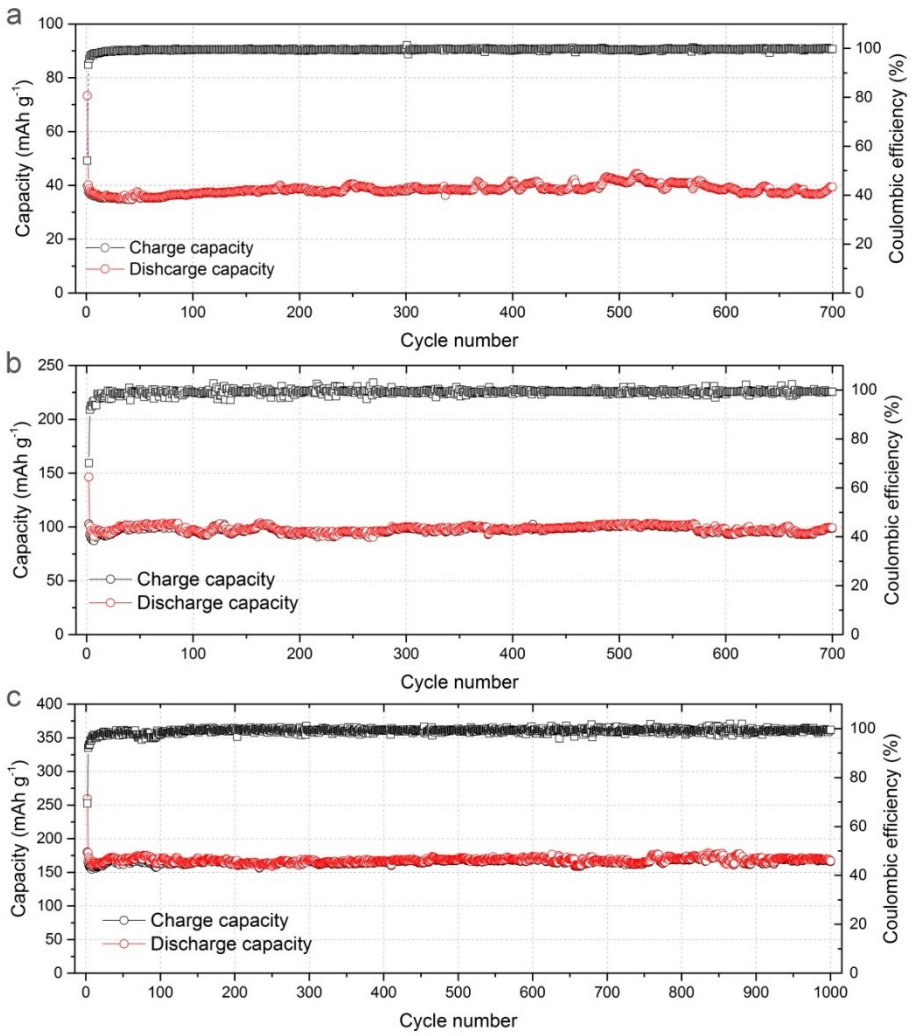

Fig. S19. Cycle performances of KTNO (a), TNO (b), and CTNO (c) at a current density of 100 mA g^{-1}.

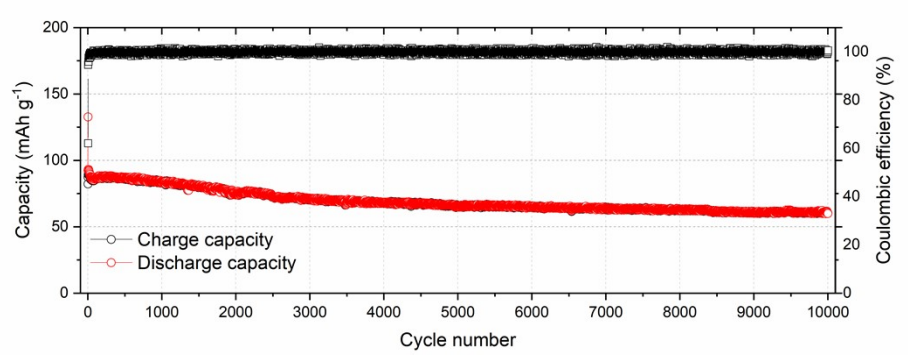

Fig. S20. Cycle performance of TNO at a current density of 1000 mA g^{-1}.

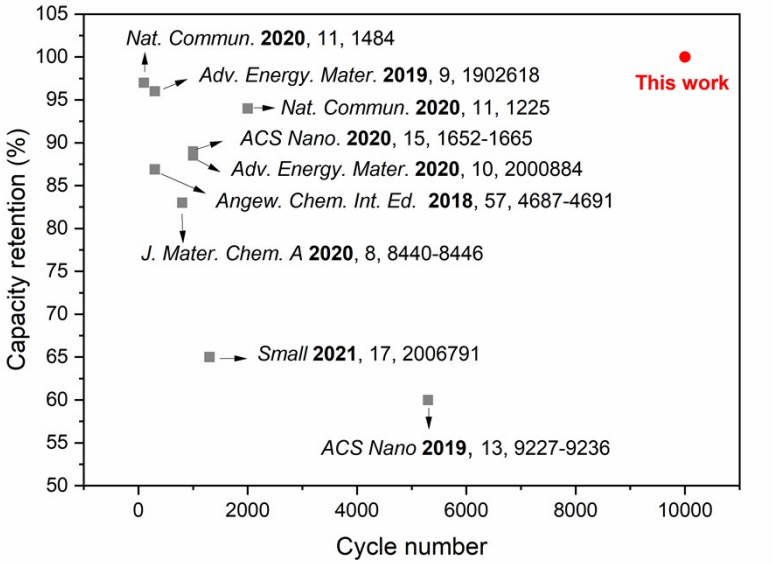

Fig. S21. Comparison of the cycle life and capacity retention for reported KIBs.

Table S1. Comparison of the electrochemical performance of reported materials in KIBs

Materials	Electrode	Capacity	Rate capability	Cycle performance	Reference
$Ti_2Nb_2O_9$	Anode	~205 mAh g^{-1} (50 mA g^{-1})	~133 mAh g^{-1} (8 A g^{-1})	10000 cycles (1A g^{-1})	**This work**
Graphite	Anode	~226 mAh g^{-1} (7 mA g^{-1})	~202 mAh g^{-1} (1.25 A g^{-1})	300 cycle (25 mA g^{-1})	**10**
Sulfur-Rich Graphene	Anode	~516 mAh g^{-1} (50 mA g^{-1})	~176 mAh g^{-1} (2 A g^{-1})	1000 cycles (2000 mA g^{-1})	**11**
P/C	Anode	~590 mAh g^{-1} (50 mA g^{-1})	~258 mAh g^{-1} (1 A g^{-1})	400 cycles (500 mA g^{-1})	**12**
Bi/C	Anode	~338 mAh g^{-1} (500 mA g^{-1})	~289 mAh g^{-1} (6 A g^{-1})	1000 cycles (5000 mA g^{-1})	**13**
Porous Bi	Anode	~400 mAh g^{-1} (200 mA g^{-1})	~322 mAh g^{-1} (1.2 A g^{-1})	300 cycles (800 mA g^{-1})	**14**
Sb	Anode	~381 mAh g^{-1} (100 mA g^{-1})	~100 mAh g^{-1} (5 A g^{-1})	200 cycles (500 mA g^{-1})	**15**
Fe_7S_8	Anode	~502 mAh g^{-1} (50 mA g^{-1})	~277 mAh g^{-1} (1 A g^{-1})	1300 cycles (2000 mA g^{-1})	**16**
CuO	Anode	~343 mAh g^{-1} (200 mA g^{-1})	~163 mAh g^{-1} (2 A g^{-1})	100 cycles (1000 mA g^{-1})	**17**
$Bi_{0.51}Sb_{0.49}OCl$ /rGO	Anode	~360 mAh g^{-1} (100 mA g^{-1})	~319 mAh g^{-1} (1 A g^{-1})	1000 cycles (100 mA g^{-1})	**18**
$KTi_2(PO_4)_3$	Anode	~73 mAh g^{-1} (128 mA g^{-1})		100 cycles (64 mA g^{-1})	**19**
$K_2Ti_8O_{17}$	Anode	~150 mAh g^{-1} (20 mA g^{-1})	~44 mAh g^{-1} (0.5 A g^{-1})	50 cycles (20 mA g^{-1})	**20**
TiP_2O_7	Anode	~298 mAh g^{-1} (100 mA g^{-1})	~139 mAh g^{-1} (5 A g^{-1})	5300 cycles (1A g^{-1})	**21**
$K_xMnFe(CN)_6$	Cathode	~142 mAh g^{-1} (28 mA g^{-1})	~94 mAh g^{-1} (1.33 A g^{-1})	100 cycles (140 mA g^{-1})	**22**
$KTiPO_4F$	Cathode	~94 mAh g^{-1} (6.6 mA g^{-1})	~26 mAh g^{-1} (0.20 A g^{-1})	100 cycles (665 mA g^{-1})	**23**
$K_{0.65}Fe_{0.5}Mn_{0.5}O_2$	Cathode	~150 mAh g^{-1} (20 mA g^{-1})	~34 mAh g^{-1} (0.80 A g^{-1})	350 cycles (100 mA g^{-1})	**24**
P2-type $K_{0.6}CoO_2$	Cathode	~78 mAh g^{-1} (2 mA g^{-1})	~43 mAh g^{-1} (0.15 A g^{-1})	150 cycles (100 mA g^{-1})	**25**
$K_{0.5}MnO_2$	Cathode	~120 mAh g^{-1} (20 mA g^{-1})	~64.6 mAh g^{-1} (1 A g^{-1})	400 cycles (400 mA g^{-1})	**26**
$KFeC_2O_4F$	Cathode	~112 mAh g^{-1} (200 mA g^{-1})	~87 mAh g^{-1} (0.5 A g^{-1})	2000 cycles (200 mA g^{-1})	**27**

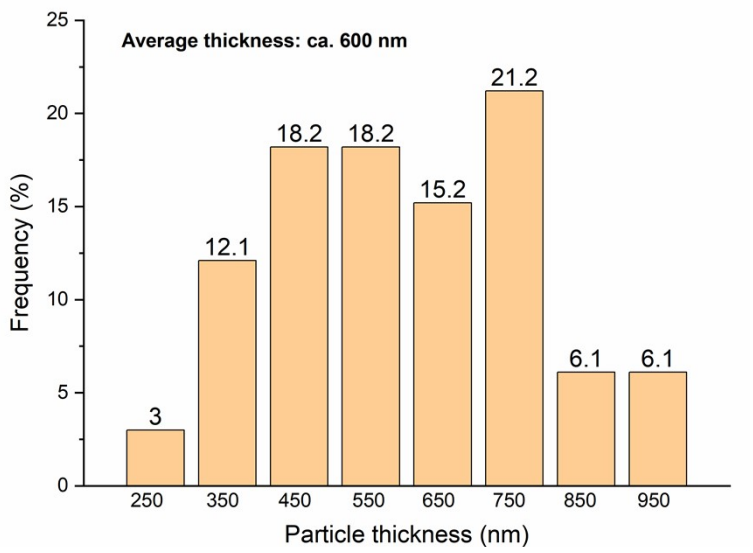

Fig. S22. Particle thickness distribution of TNO. (thickness represent the particle size along the [001] direction; data collected from the SEM images of TNO in Fig. S7c)

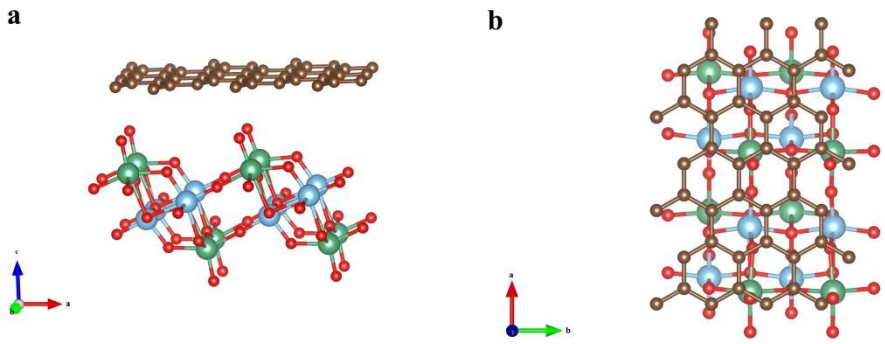

Fig. S23. The structure models of graphene-TNO from the side (a) and top (b) views.

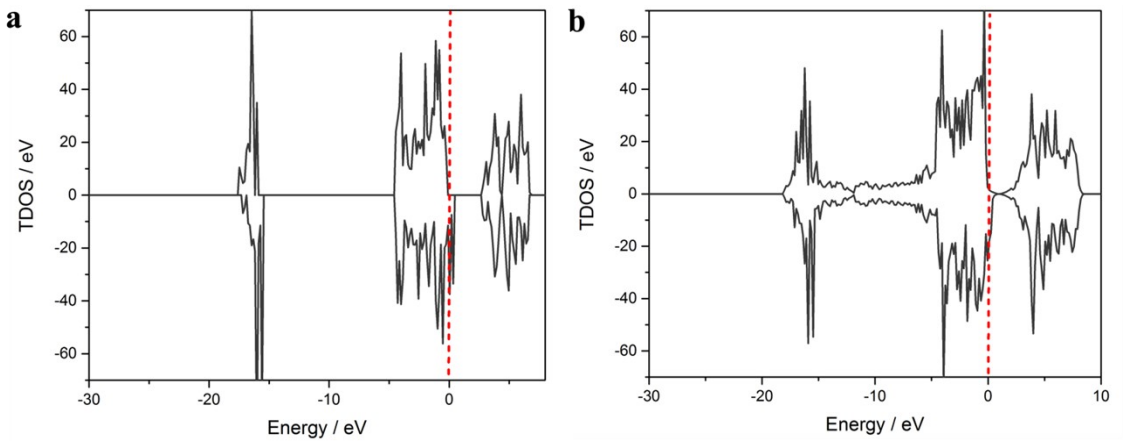

Fig. S24. Density of states of TNO (A) and graphene-TNO (B).

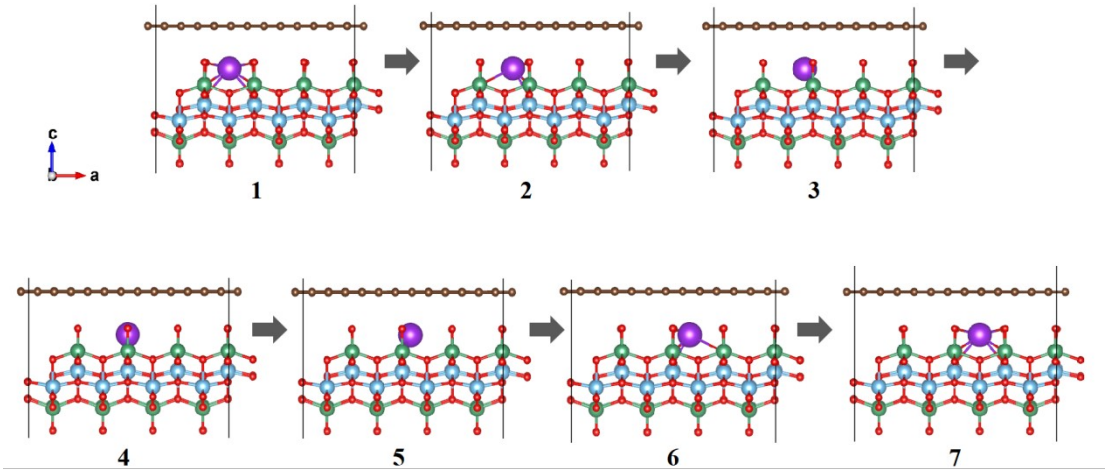

Fig. S25. The intermediate structures for the diffusion of K ion structure models for CTNO.

References

1. A. D. Wadsley, *Acta Crystallogr*. ,1964, **17**, 623-628.
2. A. Takagaki, M. Sugisawa, D. Lu, J. N. Kondo, M. Hara, K. Domen and S. Hayashi, *J. Am. Chem. Soc*., 2003, **125**, 5479-5485.
3. L. Shen, Y. Wang, H. Lv, S. Chen, P. A. van Aken, X. Wu, J. Maier and Y. Yu, *Adv. Mater*., 2018, **30**, 1804378.
4. G. Kresse and J. Furthmüller, *Phys. Rev. B*, 1996, **54**, 11169–11186.
5. J. P. Perdew, K. Burke and M. Ernzerhof, *Phys. Rev. Lett*., 1996, **77**, 3865-3868.
6. G. Henkelman, B. P. Uberuaga and H. Jónsson, *J. Chem. Phys*. 2000, **113**, 9901–9904.
7. H. Park, J. Kwon, H. Choi, T. Song and U. Paik, *Sci. Adv*., 2017, **3**, 1700509.
8. J. F. Colin, V. Pralong, M. Hervieu, V. Caignaert and B. Raveau, *Chem. Mater*., 2008, **20**, 1534-1540.
9. B. Raveau, *Revue de chimie minérale,* 1984, **21**, 391-406.
10. L. Qin, N. Xiao, J. Zheng, Y. Lei, D. Zhai and Y. Wu, *Adv. Energy Mater*., 2019, **9**, 1902618.
11. Y. Sun, H. Wang, W. Wei, Y. Zheng, L. Tao, Y. Wang, M. Huang, J. Shi, Z.-C. Shi and D. Mitlin, *ACS Nano*, 2020, **15**, 1652-1665.
12. D. Peng, Y. Chen, H. Ma, L. Zhang, Y. Hu, X. Chen, Y. Cui, Y. Shi, Q. Zhuang and Z. Ju. *ACS Appl. Mater. Interfaces,* 2020, **12**, 37275-37284.
13. T. Jiao, S. Wu, J. Cheng, D. Chen, D. Shen, H. Wang, Z. Tong, H. Li, B. Liu, J.-J. Kai, C.-S. Lee and W. Zhang, *J. Mater. Chem. A*, 2020, **8**, 8440-8446.
14. K. Lei, C. Wang, L. Liu, Y. Luo, C. Mu, F. Li and J. Chen, *Angew. Chem. Int. Ed*., 2018, **57**, 4687-4691.
15. Z. Yi, N. Lin, W. Zhang, W. Wang, Y. Zhu and Y. Qian, *Nanoscale*, 2018, **10**, 13236-13241.
16. K. Han, F. An, Q. Wan, L. Xing, L. Wang, Q. Liu, W. Wang, Y. Liu, P. Li and X. Qu. *Small*, 2021, **17**, 2006719.
17. K. Cao, H. Liu, W. Li, Q. Han, Z. Zhang, K. Huang, Q. Jing and L. Jiao, *Small*, 2019, **15**, 1901775.
18. J. Wang, B. Wang and B. Lu, *Adv. Energy Mater*., 2020, **10**, 2000884.
19. J. Han, Y. Niu, S. Bao, Y.-N. Yu, S.-Y. Lu and M. Xu, *Chem. Commun*., 2016, **52**, 11661-11664.
20. J. Han, M. Xu, Y. Niu, G.-N. Li, M. Wang, Y. Zhang, M. Jia and C. Li, *Chem. Commun*. 2016, **52**, 11274-11276.
21. Z. Li, Y. Dong, J. Feng, T. Xu, H. Ren, C. Gao, Y. Li, M. Cheng, W. Wu and M. Wu, *ACS Nano*, 2019, **13**, 9227-9236.
22. L. Xue, Y. Li, H. Gao, W. Zhou, X. Lü, W. Kaveevivitchai, A. Manthiram and J. B. Goodenough, *J. Am. Chem. Soc*., 2017, **139**, 2164-2167.
23. S. S. Fedotov, N. D. Luchinin, D. A. Aksyonov, A. V. Morozov, S. V. Ryazantsev, M. Gaboardi, J. R. Plaisier, K. J. Stevenson, A. M. Abakumov and E. V. Antipov, *Nat. Commun*., 2020, **11**, 1484.
24. T. Deng, X. Fan, J. Chen, L. Chen, C. Luo, X. Zhou, J. Yang, S. Zheng and C. Wang, *Adv. Funct. Mater*., 2018, **28**, 1800219.
25. H. Kim, J. C. Kim, S. H. Bo, T. Shi, D. H. Kwon and G. Ceder, *Adv. Energy Mater*., 2017, **7**, 1700098.
26. L. Deng, T. Wang, Y. Hong, M. Feng, R. Wang, J. Zhang, Q. Zhang, J. Wang, L. Zeng, Y. Zhu, and L. Guo, *ACS Energy Lett*., 2020, **5**, 1916-1922.
27. B. Ji, W. Yao, Y. Zheng, P. Kidkhunthod, X. Zhou, S. Tunmee, S. Sattayaporn, H.-M. Cheng, H. He and Y. Tang, *Nat. Commun*., 2020, **11**, 1225.